Monte Carlo Bethe-ansatz approach for the study of the Lieb-Liniger model

Zhe-Hao Zhang,[1,2] Yi-Cong Yu,[1,*] Yang-Yang Chen,[3,4] Song Cheng,[5,†] and Xi-Wen Guan[1,6,7]

[1]*Wuhan Institute of Physics and Mathematics, Innovation Academy for Precision Measurement Science and Technology, Chinese Academy of Sciences, Wuhan 430071, China*

[2]*University of Chinese Academy of Sciences, Beijing 100049, China*

[3]*Institute of Modern Physics, Northwest University, Xi'an 710069, China*

[4]*Shaanxi Key Laboratory for Theoretical Physics Frontiers, Xi'an 710069, China*

[5]*Beijing Computational Science Research Center, Beijing 100193, China*

[6]*Department of Theoretical Physics, Research School of Physics and Engineering, Australian National University, Canberra ACT 0200, Australia*

[7]*Peng Huanwu Center for Fundamental Theory, Xi'an 710069, China*

(Received 6 December 2023; accepted 8 March 2024; published 27 March 2024)

We have developed a Monte Carlo algorithm to explore the equilibrium and out-of-equilibrium properties of the Lieb-Liniger model. This Monte Carlo Bethe-ansatz (MCBA) algorithm has enabled us to successfully reconstruct statistical ensembles for equilibrium or postquench dynamics, thereby facilitating the calculation of macroscopic quantities of integrable models. Our results substantiate the validity of the (quench) thermodynamic Bethe-ansatz equation from the perspective of first-principles statistical physics. Additionally, we have employed this method to study the generalized Gibbs ensemble in relation to the postquench dynamics of the Lieb-Liniger model. Furthermore, we have demonstrated the MCBA algorithm's capacity to calculate correlations using Bethe-ansatz wave functions. Our approach offers an efficient methodology for the investigation of the equilibrium and out-of-equilibrium properties of integrable systems.

DOI: 10.1103/PhysRevA.109.033320

I. INTRODUCTION

The description of equilibrium and out-of-equilibrium properties in isolated quantum many-body systems within the framework of statistical mechanics is a fundamental open question [1–5]. It has been widely accepted that although the entire system remains in a pure state, the reduced density matrix of an arbitrary finite compact subsystem can be described by a statistical ensemble in the long-time limit [6,7]. Furthermore, in generic isolated systems, nonequilibrium dynamics are expected to result in thermalization, where the values of macroscopic quantities become stationary and predictable by statistical mechanics, irrespective of the widely differing initial states [3,8,9]. Over the past few decades, the experimental capability to investigate almost purely unitary time evolution in cold atoms [10–20] has led to considerable theoretical excitement, significantly enhancing our understanding of equilibrium and evolution of many-body quantum systems [4–7,21–41].

One of the leading principles underlying the dynamics of isolated quantum systems out of equilibrium is that of the transport carried by conserved currents, particularly for those emerging from unitary evolutions [31,42]. Consequently, the real-time dynamics of integrable models, which possess an infinite number of conservation laws leading to generalized thermalization [26,43,44], serves as a paradigm to study the dynamics out of equilibrium [31,45]. It has been proposed that integrable models equilibrate to generalized Gibbs ensembles (GGE) involving higher conserved charges of the systems [33,45–47]. The investigation of GGE has been a central topic in the study of the dynamics of integrable models over the past decade [21,24,25,45], including the rigorous proof of the emergence of the GGE in certain noninteracting theories [6,22,33] and the observation of the signs of the GGE on experimental platforms [20,48–54]. The key idea of these studies is the utilization of general statistical physics methods in the investigation of nonequilibrium quantum systems through the study of statistical ensembles [55,56].

On the other hand, the quantum Monte Carlo method (QMC), whose effectiveness has been demonstrated in numerous studies of various quantum systems [57–62], is a traditional and significant tool for investigating quantum many-body physics [63,64]. The underlying reason enabling the implementation of QMC is its ability to accurately and efficiently sample a well-defined distribution on an artificially introduced "phase space," which is derived from the original quantum problems through a variety of ingenious methods [59,65,66]. This process can also be regarded as a simulation of statistical ensembles which is just a phase space with a well-defined probability distribution. In a more specific context, the implementation of the Monte Carlo method involves generating a Markov chain of points in the phase space based on the given probability distribution, and this sampling method is known as the Metropolis algorithm [67].

*ycyu@wipm.ac.cn
†scheng@csrc.ac.cn

Once the generated Markov chain reaches thermalization, the set of states it generates can faithfully represent the statistical ensemble. When the ensembles are simulated, it is possible to approximate and analyze the macroscopic and microscopic properties of quantum systems, overcoming the computational challenges posed by the many-body problem [66].

The inherent mechanism of QMC naturally leads to the following idea: for a statistical ensemble of an exactly solvable model, in principle, we clearly know the analytical form of the wave function of each state and its corresponding probability, so we could solve the equilibrium and evolution of the system by directly constructing the statistical ensemble. This idea motivates our research.

This paper is arranged as follows. In Sec. II, we introduce the Monte Carlo Bethe-ansatz method (MCBA), and prove through examples that it can calculate the thermodynamic quantities for systems in equilibrium by comparing with exact solutions. In Sec. III, we further investigate the quench dynamics of integrable systems using the algorithm developed in Sec. II, and discuss the problem related to the GGE. In Sec. IV, by constructing a new statistical ensemble, we extended the Monte Carlo method to the calculation of wave functions in an integrable model. We give a summary and outlook in Sec. V.

II. THE MONTE CARLO BETHE ANSATZ

Traditionally, the QMC method (for instance, the variational quantum Monte Carlo [58,59]) works by representing the wave function with a set of random walkers, each of which represents a possible configuration (wave function) of the system [55,66]. These walkers are propagated using a Metropolis algorithm, which generates new configurations of the system according to the probability associated with each configuration. From a physics perspective, the random walkers construct an ensemble corresponding to a known distribution.

For the simplest case in statistical physics, the canonical ensemble, we can write down the corresponding probability a_n assigned to each $|\psi_n\rangle$ by

$$a_n = \frac{1}{Z} e^{-\beta \langle \psi_n | \hat{H} | \psi_n \rangle}, \tag{1}$$

where $\hat{H}$ is the Hamiltonian, $\beta = (k_B T)^{-1}$ is the inverse temperature with T being the temperature and k_B the Boltzmann constant, and Z is the partition function given by $Z = \sum_n e^{-\beta \langle \psi_n | \hat{H} | \psi_n \rangle}$. The effectiveness of the QMC method comes from its ability to represent the statistical ensembles, and thus it can provide thermodynamic information of a system in equilibrium [56]. For algorithm correctness, the random walkers $|\psi_n\rangle$ must form a complete basis of the Hilbert space; they are chosen to be the Vannier basis in lattice models or the eigenvectors of a noninteracting Hamiltonian, conventionally, for the sake of computational simplicity. Evidently, the $|\psi_n\rangle$ can also be selected as the eigenvector of the Hamiltonian of the system, giving rise to the idea of the MCBA [68–71]. The benefit of this approach is that in the integrable models with exact solutions, the eigenvalues and the corresponding eigenvectors can be solved analytically, and thus the probability in (1) can be analytically calculated in principle.

In the following discussion, we will use the Lieb-Liniger model as a playground to discuss the MCBA algorithm. The Lieb-Liniger model (LLM) [72,73] is one of the extensively studied quantum integrable models, which provides an excellent description of the properties of one-dimensional Bose gas [74]. We use the LLM as the example to discuss the MCBA algorithm for the following reasons: Firstly, the Bethe-ansatz equations (BAE) for the LLM are relatively simple, especially in the case of repulsive interaction, where all the roots of the BAE are real, facilitating our numerical calculations. Secondly, the MCBA method can demonstrate its advantages in handling continuous models, which is not trivial to deal with numerically.

A. The Lieb-Liniger model

The LLM describes a system with N indistinguishable bosons subject to a delta-function pairwise interaction potential in a periodic one-dimensional (1D) geometry with size L. It was first solved through Bethe ansatz (BA) by Lieb and Liniger [72,73], and the detailed discussion of the BA approach to LLM can be found in Refs. [74,75]. The first-quantized Hamiltonian for this system can be written as

$$\hat{H} = -\sum_{i=1}^{N} \frac{\partial^2}{\partial x_i^2} + 2c \sum_{i<j} \delta(x_i - x_j), \tag{2}$$

where we work in the unit setting $\hbar = 2m = 1$. From this point forward, we will discuss the repulsive case ($c > 0$). The exact eigenstates of (2) under periodic boundary conditions $\Psi(\dots, x_j, \dots) = \Psi(\dots, x_j + L, \dots)$ are BA wave functions

$$\Psi(x_1, x_2, \dots, x_N) = \sum_{P \in S_N} A(P) \prod_{j=1}^{N} e^{i k_{P_j} x_j}, \tag{3}$$

with S_N in (3) denoting the permutation group of degree N, and the amplitudes

$$A(P) = \exp\left[i \sum_{1 \leqslant i < j \leqslant N} \arctan \frac{c}{k_{P_i} - k_{P_j}} \right]. \tag{4}$$

Notice that the form (3) is solely valid within the confined sector $x_1 < x_2 < \cdots < x_N$, while the value of the wave function in other sectors can be obtained by its symmetric property. The rapidities $\boldsymbol{k} \triangleq \{k_1, k_2, \dots, k_N\}$ are solutions of the BAE [72]

$$L k_j = 2\pi I_j - 2 \sum_{k=1}^{N} \arctan \frac{k_j - k_k}{c} \tag{5}$$

for $j = 1, 2, \dots, N$. The set of "quantum numbers" $\boldsymbol{I} \triangleq \{I_1, I_2, \dots, I_N\}$ determines the solutions of the BAE (5), which are integers (half-integers) for N odd (even) numbers under the constrain

$$I_1 < I_2 < \cdots < I_N. \tag{6}$$

Moreover, the eigenenergy of a certain BA wave function in (5) is determined by

$$E_{\boldsymbol{I}} = \sum_{j=1}^{N} [k_j(\boldsymbol{I})]^2. \tag{7}$$

B. The algorithm

The canonical ensemble $\mathcal{E}_{\rm LLM}$ of the LLM at (inverse) temperature β can be constructed directly from the BA solution introduced in Sec. II A, composed by any eigenfunction of (2) with a probability $a_{\boldsymbol{I}} = e^{-\beta E_{\boldsymbol{I}}}/\sum_{\boldsymbol{I}} e^{-\beta E_{\boldsymbol{I}}}$. Notice that a quantum number $\boldsymbol{I}$ under condition (6) must uniquely correspond to an eigenfunction of the Hamiltonian (2) in its Hilbert space, thus the ergodicity of the eigenstates in $\mathcal{E}_{\rm LLM}$ can be achieved by the random walk of the quantum number $\boldsymbol{I}$. Based on this observation, we design a Metropolis algorithm as follows.

Initialization. The random walker begins with an initial quantum number $\boldsymbol{I}_{\rm ini}$, and customarily we set $\boldsymbol{I}_{\rm ini} = \{-\frac{N-1}{2}, -\frac{N-1}{2}+1, \ldots, \frac{N-1}{2}\}$ as the quantum number of the ground state.

Random walk. We utilize the Metropolis algorithm to implement quantum walks in the canonical ensemble. Let j loop from 1 to N, we ask $I_j \in \boldsymbol{I}$ undergo a random walk, and the rule is designed as the following: first, we randomly generate a candidate $I_j^c = I_j \pm 1$, each with 50% probability, i.e., the candidate walker $\boldsymbol{I}^c$ differs from the current walker $\boldsymbol{I}$ only by the jth component. Next, we check the validity of the condition (6): if (6) does not hold, we reject the candidate $\boldsymbol{I}^c$, the random walker remains unchanged; else we calculate the current energy $E_0 = E_{\boldsymbol{I}}$ and the candidate energy $E = E_{\boldsymbol{I}^c}$ by (7), and simultaneously generate a random number p with a uniform distribution between 0 and 1. Based on the Metropolis algorithm, we accept the candidate $\boldsymbol{I}^c$ if $p < e^{\beta(E_0-E)}$, and reject it otherwise.

Analysis. From the random walk designed above we obtain a Markov chain $\boldsymbol{I}_n$ for $n = 1, 2, \ldots$. We can estimate the thermalization time $n_{\rm th}$ of this random process by calculating physical observables,—for instance, the energy (7). Next, we use the random walkers $\boldsymbol{I}_n$ for $n > n_{\rm th}$ to construct an ensemble $\mathcal{E}_{\rm MC}$, and it can be proved that $\mathcal{E}_{\rm MC} \to \mathcal{E}_{\rm LLM}$ when the size of $\mathcal{E}_{\rm MC}$ goes to infinity [63,65]. Finally, all the thermodynamic quantities of the system can be approximately calculated by this generated ensemble $\mathcal{E}_{\rm MC}$.

We name the algorithm introduced above Monte Carlo Bethe ansatz (MCBA) as it is a typical Monte Carlo method based on the Bethe-ansatz solutions. Our calculations confirm the thermalization properties of the MCBA in Fig. 1, proving its validity. Quick thermalizations are observed. Due to the finite size effect, the energy densities in equilibrium in Figs. 1(a)–1(c) differ slightly from the result $E/L = 0.9024$ obtained by the TBA equations, which is derived in the thermodynamic limit $L \to \infty$. We also observe that the thermalization time $n_{\rm th}$ grows linearly with system size, confirming the scalability of the algorithm. Please note that the MCBA algorithm is a first-principles computation; it is based on the fundamental principles of statistical physics, without any additional approximations. In the following subsection, we will use the MCBA algorithm as a benchmark to verify the validity of the Yang-Yang thermodynamic method [76],

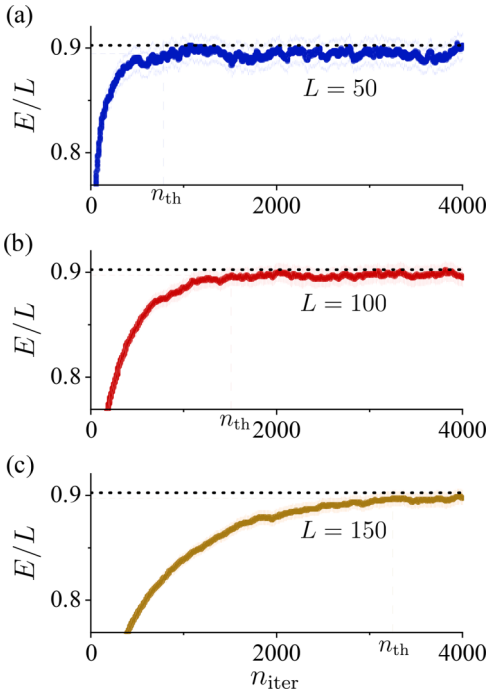

FIG. 1. The thermalization of the MCBA method for the LLM. We set $T = 1.0$, $c = 1.0$, and $N/L = 1.0$, referring to the unit density. (a)–(c) correspond to the system size $L = 50$, 100, and 150, respectively. The horizontal axis refers to the iterations, each iteration completes a scan from 1 to N in the algorithm introduced in the text, and vertical axis refers to the energy density. The black dash lines present the numerical result of the energy density via thermodynamic Bethe-ansatz equation (9), giving $\lim_{L\to\infty} E/L = 0.9024$, and the colored dot lines correspond to the results from MCBA. In this approach we take 500 random walkers; the solid line is the mean value of the random walkers while the shadowed areas correspond to the error bars with 99.7% confidence level. n_t denotes the thermalization time, defined by the first time that the mean value calculated by all the random walkers reaches the result of long-time average. The results show the validity of the MCBA. The random walkers reach the equilibrium states quickly and the variances decay with the increase of the system size.

which is an important method extensively used for calculating the thermodynamic properties of integrable models [77].

C. The reconstruction of the Yang-Yang ensemble

1. The Yang-Yang thermodynamics

The thermodynamic properties of the LLM were first analytically studied by C. N. Yang and C. P. Yang in 1969 by the statistical method named Yang-Yang thermodynamics [76], which led to a significant step in studying the macroscopic properties of integrable systems in an exact manner and provided profound understanding to a variety of physical phenomena, such as universal thermodynamics, quantum criticality, and Luttinger liquids [74,77]. The key idea behind the Yang-Yang thermodynamics is to perform coarse-graining on the grand canonical ensemble $\mathcal{E}_{\rm LLM}$ to obtain an ensemble $\mathcal{E}_{\rm YY}$ called the Yang-Yang grand canonical ensemble in the thermodynamic limit. Each state in $\mathcal{E}_{\rm YY}$ is labeled by a distribution function $\rho(k)$ in the rapidity space. Explicitly, a

state labeled by $\boldsymbol{I}$ in $\mathcal{E}_{\rm LLM}$ is mapped onto a state in $\mathcal{E}_{\rm YY}$ through $\boldsymbol{I} \to \boldsymbol{k} \to \rho(k)$, where the first mapping is the solving of the BAE (5), and the second one is the density estimation. Because this mapping is many-to-one, each state in $\mathcal{E}_{\rm YY}$ is equipped with an effective entropy [32,76,78]

$$\frac{S}{L} = \int dk[(\rho+\rho^h)\ln(\rho+\rho^h) - \rho\ln\rho - \rho^h\ln\rho^h], \quad (8)$$

where $\rho^h(k)$ is the hole density which can be also obtained by solving the BAE, see Ref. [75] for details. The grand canonical thermal potential can be written as $\Omega = E - TS - \mu N$, and $\delta\Omega = 0$ gives the thermodynamic Bethe-ansatz equation (TBA)

$$\epsilon(k) = k^2 - \mu - \int dk' a_2(k-k') T \ln[1+e^{-\epsilon(k')/T}], \quad (9)$$

where $\epsilon(k)$ is the dressed energy defined by $\epsilon(k) = T\ln[\rho^h(k)/\rho(k)]$, and the kernel $a_2(k) = \frac{1}{2\pi}\frac{2c}{k^2+c^2}$. The solution of (9), together with the integral relation [75]

$$\rho(k) + \rho^h(k) = \frac{1}{2\pi} + \int dk' a_2(k-k')\rho(k'), \quad (10)$$

determines the density $\rho(k)$, which corresponds to the maximum weight state in the $\mathcal{E}_{\rm YY}$, providing the thermodynamic properties of the LLM.

2. The $\rho(k)$ generated by MCBA

Notably, the function $\rho(k)$ can be numerically obtained via MCBA by averaging all the random walkers $\boldsymbol{I}$ in $\mathcal{E}_{\rm MC}$ through the mapping $\boldsymbol{I} \to \boldsymbol{k} \to \rho(k)$. In each step of the random walk we record the solution $\boldsymbol{k}$ of the BAE (5), these ks forms a large set of k, and finally we can obtain a density distribution $\rho(k)$ by discretization. As an intermediate variable for calculating physical quantities, the $\rho(k)$ obtained by MCBA shares the same formula as the one obtained by TBA, thus we can regard the generation of the $\mathcal{E}_{\rm MC}$ by the random walker as the reconstruction of the Yang-Yang ensemble $\mathcal{E}_{\rm YY}$; see discussion in Sec. III C.

In Figs. 2(a) and 2(b) we present the comparisons between the results from the TBA and the MCBA in different temperatures. The results show that the MCBA and TBA are in good agreement, even though the system size in MCBA is not large ($L = 100$). Here, we set $n = N/L = 1.0$, thus the distribution $\rho(k)$ is normalized. The density function $\rho_{\rm MC}(k)$ obtained by the MCBA converges to the function $\rho_{\rm TBA}(k)$ obtained by TBA quickly when the system size L grows; we show the scaling behavior of the error defined by $f_{\rm err} = \int_{-\infty}^{\infty} dk|\rho_{\rm MC}(k) - \rho_{\rm TBA}(k)|^2$ in Fig. 2(c). These calculations prove the reliability and effectiveness of the MCBA, and the well-behaved scaling property guarantees that we can approximate the thermodynamic limit results by performing calculations on a relatively small system size through MCBA. This advantage may potentially lead to more applications, such as studying thermodynamics properties in the integral models where TBA equations have not been established yet (the Richardson-Gaudin model [79] or central spin model [80], for instance), or studying the integral models where TBA equations are difficult to handle (multicomponent Bose gas [81,82], for example). We hope to explore this research direction in our future works.

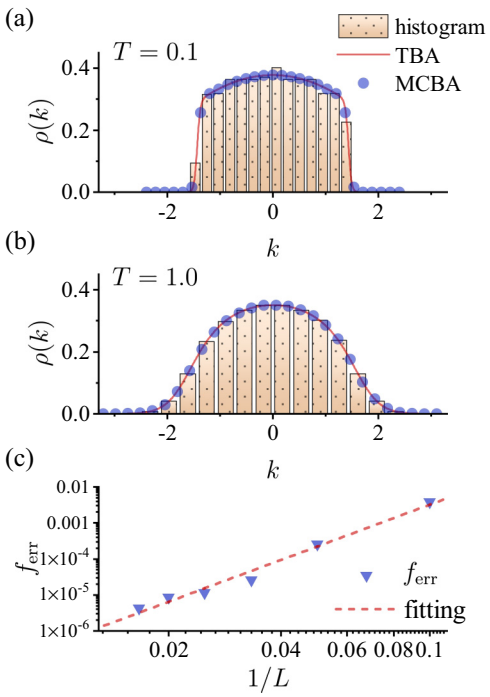

FIG. 2. The reconstruction of the $\mathcal{E}_{\rm YY}$ by MCBA. In (a) and (b) the red solid lines are obtained by solving the TBA (9) numerically, the histograms are obtained by the data generated by the MCBA, and the blue dots are obtained by the kernel density approximation of the data. The results from MCBA closely match the results from numerical solutions of the TBA. Here in (a) and (b), we set $L = 100$, $N/L = 1.0$, $c = 1.0$, and $T = 0.1$ and 1.0 respectively, and the total number of samplings are both 1×10^5. In (c) we present the scaling behavior of the distance between the results from MCBA and TBA defined by $f_{\rm err} = \int_{-\infty}^{\infty} dk|\rho_{\rm MC}(k) - \rho_{\rm TBA}(k)|^2$, using the data generated at $T = 1.0$. Fast convergence is observed when the system size grows.

III. THE STUDY OF QUENCH DYNAMICS via MCBA

The success of Yang-Yang thermodynamics lies not only in its description of the equilibrium state of many-body systems, but more importantly, it also gives an impetus for recent developments on generalized hydrodynamics and quantum transport of quantum integrable systems of interacting spins [24,30,71], bosons, and mixtures. It was proposed that for a postquench integrable model, the behavior of local observables at late time can be given by the expectation values with respect to a single Hamiltonian eigenstate [23,32]. This fact can be regarded as a generalization of the eigenstate thermalization hypothesis, and it can also be considered as a generalization of the saddle-point approximation in the derivation of the TBA equation (9), which claims that the statistical properties can be well described by the states with maximum weight in the Yang-Yang ensemble $\mathcal{E}_{\rm YY}$. To be explicit, let $\{|\psi_m\rangle\}$ be a complete set of eigenstates of the Hamiltonian, i.e., $\hat{H}|\psi_m\rangle = E_m|\psi_m\rangle$; the time evolution of an arbitrary initial state $\Psi(0)$ is then given by

$$|\Psi(t)\rangle = \sum_m a_m e^{-iE_m t}|\psi_m\rangle, \quad (11)$$

where $a_m = \langle\psi_m|\Psi(0)\rangle$ is the overlap between the initial state and the mth eigenstate. The long-time average of an observable $\hat{O}$ in a finite volume case can be written as

$$\lim_{\tau\to\infty}\frac{1}{\tau}\int_0^\tau dt\langle\Psi(t)|\hat{O}|\Psi(t)\rangle = \sum_m |a_m|^2\langle\psi_m|\hat{O}|\psi_m\rangle. \quad (12)$$

The right-hand side of this equation can be interpreted as a statistical ensemble called the diagonal ensemble (DE), in which the weight of the eigenstate $|\psi_m\rangle$ is determined by $|a_m|^2$. The system thermalizes if the DE gives the same physical predictions as a canonical or grand canonical ensemble, which is expected for a nonintegrable model. However, in an integrable model the existence of a large number of higher conserved charges prevents thermalization. It was suggested that in integrable models the DE predictions should agree with those of a generalized Gibbs ensemble, whose density matrix is defined as

$$\hat{\rho}_{\rm GGE} = \frac{\exp\big(-\sum_j \beta_j\hat{\mathcal{I}}_j\big)}{\mathrm{Tr}\big[\exp\big(-\sum_j \beta_j\hat{\mathcal{I}}_j\big)\big]}, \quad (13)$$

where the $\hat{\mathcal{I}}_j$ are some conserved operators and β_j are the corresponding Lagrangian multipliers [32,33,38,45,83]. Equation (13) is a generalization of the ensembles we often meet in statistical physics. For instance, for the canonical ensemble we have only one $\beta_0 = 1/(k_{\rm B}T)$, $\hat{\mathcal{I}}_0 = \hat{H}$, and for the grand canonical ensemble, we have extra $\beta_1 = \mu$, $\hat{\mathcal{I}}_1 = \hat{N}$, denoting the chemical potential and particle number operator. It was proposed firstly in Ref. [43] that the relaxation of the hardcore bosons, which is a completely integrable many-body quantum system, can be described by GGE, and in subsequent work, researchers have confirmed the feasibility of this idea across a range of models. It has been proved analytically that the stationary postquench properties in the one-dimensional Bose gas can be well described by the GGE [22,84]; furthermore, in the specific Heisenberg spin chain model [26], researchers were able to directly construct the operators $\hat{\mathcal{I}}_j$ in (13) by algebraic Bethe ansatz. It has also been found that the GGE emerges in the bosonic postquench Aubry-André model at the nonlocal and critical states [47], and it also governs the dynamics of the perturbed LLM by a one-body parabolic trap [21]. These works to some extent demonstrate the robustness and universality of the GGE.

However, as research progressed and a series of integrable models were rigorously studied, it was discovered that in some cases, the straightforwardly constructed GGE cannot provide a complete description of the steady states of the quantum integrable systems. It was proved that in the XXZ model, the GGE failed to give the accurate postquench behavior from an equilibrium state, especially when considering the correlators [24,25]. The same phenomenon has also been observed in the study of Bose gas [29,83]. In these cases, researchers are able to obtain analytical results for the overlap integrals between the initial states of the system and the eigenstates of the quenched Hamiltonian, which enables the study of the DE of the system after long-time evolution and the comparison to the GGE results. The key to this analytical approach lies in analogizing the overlap integrals obtained, denoted as $a_n = \langle\psi_n|\Psi(0)\rangle$, with the statistical ensemble, as represented in (1). By introducing a new action derived from the overlap integrals, known as the *quench action*, one can describe the diagonal ensemble effectively within the framework of traditional statistical physics [23,32,71,85].

In this section, we will approach the connection between the DE and the GGE from a different perspective. Unlike previous studies that compare the DE and GGE through computational results [21,24,25,29,83], our research aims to directly construct the DE described by Eq. (12) using Monte Carlo sampling methods. We will analyze the properties of this ensemble using large datasets to address the relation to the GGE.

A. The MCBA for quench action

We study the quench dynamics from the ground state $|0\rangle$ [the Bose-Einstein condensate (BEC) state] of the noninteracting LLM to the interacting one, which was discussed in detail in a series of works [29,32,83]. It was proved numerically that the long-time behavior of LLM can be well described by the DE according to the validity of Eq. (12) even in a small system size [29]. Considering the Hamiltonian (2) with even N, only the parity-invariant Bethe-ansatz states $|\vec{k},-\vec{k}\rangle \triangleq |\{k_j\}_{j=1}^{N/2}\cup\{-k_j\}_{j=1}^{N/2}\rangle$ with k_j being positive and $\{k_j\}_{j=1}^{N/2}\cup\{-k_j\}_{j=1}^{N/2}$ being the solution of the BAE (5) have nonzero overlap with the initial BEC state $|0\rangle$. The overlap formula is given by [32,83,86]

$$\langle\vec{k},-\vec{k}|0\rangle = \sqrt{\frac{(cL)^{-N}N!}{\det[\boldsymbol{G}]}}\frac{\det[\boldsymbol{G}^{\boldsymbol{Q}}]}{\prod_{j=1}^{N/2}\frac{k_j}{c}\sqrt{\frac{k_j^2}{c^2}+\frac{1}{4}}}, \quad (14)$$

where the $\boldsymbol{G}$ and $\boldsymbol{G}^{\boldsymbol{Q}}$ are Gaudin matrices with elements $G_{jm} = \delta_{jm}[L+\sum_{l=1}^{N}K(k_j,k_l)] - K(k_j,k_m)$, $j,m = 1,\ldots,N$ and $G^{Q}_{jm} = \delta_{jm}[L+\sum_{l=1}^{N/2}K^{Q}(k_j,k_l)] - K^{Q}(k_j,k_m)$, $j,m = 1,\ldots,N/2$, with the functions $K(k,\mu) = 2c/[c^2+(k-\mu)^2]$ and $K^{Q}(k,\mu) = 2c/[c^2+(k-\mu)^2] + 2c/[c^2+(k+\mu)^2]$. Taking the probability represented by $|\langle\vec{k},-\vec{k}|0\rangle|^2$ compared to the probability represented by $Z^{-1}\exp[-\beta E(\vec{k})]$ in the canonical ensemble, we can follow the idea in Ref. [76] to derive the TBA equations using the coarse-graining method and saddle-point approximation. This derivation was discussed in detail in Refs. [83] and [32], and we present only the final result,

$$\epsilon(k) = \log\left[\frac{k^2}{c^2}\left(\frac{k^2}{c^2}+\frac{1}{4}\right)\right] - h - \int_{-\infty}^{\infty}a_2(k-p)\ln[1+e^{-\epsilon(p)}]dp, \quad (15)$$

where similarly $\epsilon(k) = \ln[\rho^h(k)/\rho(k)]$ with $\rho(k)$ and $\rho^h(k)$ being the particle and hole density, respectively. Notice that (15) is similar to (9) except for the driving term, and the extra Lagrangian multiplier h in (15) can be determined by the density.

In Sec. II we showed the validity and effectiveness of the MCBA in equilibrium, which relies on its ability to represent the Yang-Yang ensemble. This encourages us to apply the same method to study the postquench DE. By making slight modifications to the algorithm, replacing the

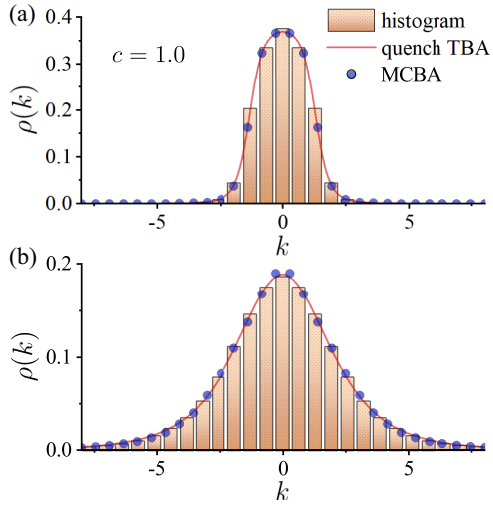

FIG. 3. The reconstruction of the DE after quench by MCBA. In (a) and (b) the histograms are obtained by the data generated by the MCBA, the red solid lines are obtained by solving the quench TBA (9) numerically, and the blue dots are obtained by the kernel density approximation of the data. The results from MCBA closely match the results from numerical solutions of the TBA. Here in (a) and (b), we set $L = N = 50$, and $c = 1.0$ and 10.0, respectively. The total number of samplings are both 2×10^5.

probability $Z^{-1}\exp[-\beta E(\vec{k})]$ with the probability $|\langle\vec{k}, -\vec{k}|0\rangle|^2$ in the Metropolis random walk, we can reconstruct the postquench DE numerically.

In Fig. 3, we present the results of our MCBA algorithm and compare them to the quench TBA equation. We find that the results of the quench TBA equation can be obtained for relatively small system sizes $N = L = 50$, similar to the canonical ensemble case in Sec. II. The scatter points in Fig. 3 are obtained by the kernel density approximation from the datasets generated by the MCBA, which match well with the quench TBA equation (15).

We emphasize that our method are fundamentally different from the calculations based on the (quench) TBA equations. The derivation of (quench) TBA equations requires two important additional assumptions in addition to the fundamental principles in statistical physics. The first one comes from the form of the Yang-Yang entropy (8), which is rooted in the quasi-particle picture of Landau's Fermi liquid theory [78]. In this picture, a coarse-graining method in momentum space is effective; however, in the corresponding BAE, it is necessarily assumed that local particle-hole excitations at the Bethe roots, at least statistically, do not affect the overall distribution of them. The second assumption is the saddle-point approximation [87], which involves finding the state with the highest probability in the ensemble and using it to represent the entire ensemble in calculations. In contrast to (quench) TBA, the MCBA method is first-principles-based, relying solely on the results from exact solutions [(7) and (14)] and fundamental principles of statistical physics [(1) and (12)], without any additional assumptions. Thus, in this sense, our results in Figs. 2 and 3 provide a numerical validation of the effectiveness of the (quench) TBA equations (9) and (15).

B. The construction of the GGE

The MCBA method described in Sec. III A can generate a diagonal ensemble of the postquench LLM, and we also know the probabilities associated with each state $|\vec{k}, -\vec{k}\rangle$ in this ensemble as $P(\vec{k}) = |\langle\vec{k}, -\vec{k}|0\rangle|^2$. Suppose that the DE can be described by the GGE; this means that the probability $P(\vec{k})$ can be well fitted by

$$P(\vec{k}) \propto e^{-\sum_m \beta_m \mathcal{I}_m(\vec{k})} \tag{16}$$

with $\mathcal{I}_m(\vec{k}) = \langle\vec{k}|\hat{\mathcal{I}}_m|\vec{k}\rangle$.

For the LLM, which can be obtained from quantizing the nonlinear Schrödinger equation, a series of its conserved quantities can be derived by expansion of the trace of its monodromy matrix; please refer to Chap. 2 in Ref. [75] and Ref. [88] for details. Although higher-order conserved quantities have highly complicated algebraic forms [88], their mutual commutativity allows us to combine them into a series of commutative $\hat{\mathcal{I}}_m$ operators. These operators have the property that their expectation values on a Bethe-ansatz state are equal to the mth power sum of the N Bethe roots corresponding to that state [31,89], i.e.,

$$\langle\vec{k}|\hat{\mathcal{I}}_m|\vec{k}\rangle = \mathcal{I}_m(\vec{k}) = \sum_{j=1}^{N} k_j^m. \tag{17}$$

Obviously, $\hat{\mathcal{I}}_0 = \hat{Q}, \hat{\mathcal{I}}_1 = \hat{P}$, and $\hat{\mathcal{I}}_2 = \hat{H}$ correspond to the particle number, momentum, and energy respectively.

A simple idea is that we can construct a generalized Gibbs ensemble with these conserved quantities, so that this ensemble can approach the postquench diagonal ensemble, with the additional requirement that the number of these conserved quantities is finite [90] (otherwise, a theory with an infinite number of parameters lacks predictive power). This means that the probability on the left-hand side of (16) can be well approximated by its right-hand side with the expression of $\mathcal{I}_m$ in (17), but when we attempted to numerically fit the states in the DE obtained through the MCBA method in the form of the right-hand side of (16) we failed, and we even found that using more conserved quantities does not provide substantial help in reducing the fitting error. However, it was widely regarded that the GGE, when implemented correctly, should converges to the quench action ensemble (which is equivalent to the DE) in the thermodynamic limit [32]; this suggests that the sequence of conserved quantities we obtained through the quantum inverse scattering method should not be equated with the sequence of conserved quantities in the GGE (13), at least in the model we are studying. This confirms the conclusions in Refs. [83,91] and [29] that simply using the GGE does not yield the correct results.

However, the conserved quantities that satisfy the requirements of the GGE, i.e., the condition (16), can be obtained in a simple way. Following the reasoning behind the quench action derivation presented in Refs. [32] and [83], we observe that in the overlap given by (14), the $\boldsymbol{G}^{\boldsymbol{Q}}$ and $\boldsymbol{G}$ matrices in the numerator and denominator can be approximated by $L(\mathrm{id})$ in the thermodynamic limit $L \to \infty$, so their determinants approach $L^{N/2}$ and L^N, respectively. The second-order correction is of the order $O(\frac{1}{L})$, which can be safely ignored in the thermodynamic limit. This inspires us to make the following

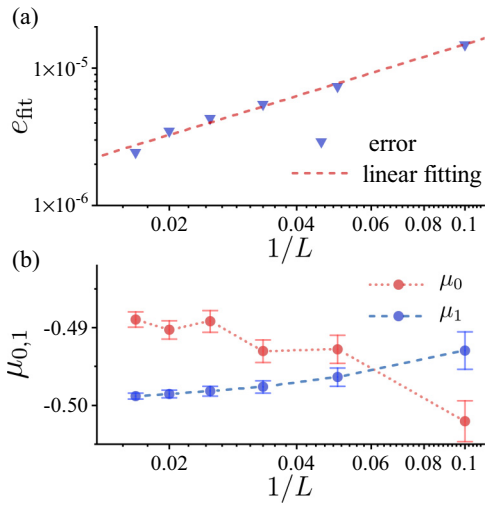

FIG. 4. The fitting of the postquench DE by (18) by the conjecture form (19) with different system sizes. (a) The fitting error vs the system size. The error is expressed as the variance of the error of 2×10^3 samples. Our result shows that the fitting error decreases exponentially with the increase of system size. (b) The fitting result of the effective chemical potential μ_1 and μ_2 in (18), where μ_0 serves as a renormalizing constant, and the μ_1 corresponds to the operator (23). The result shows that μ_1 approaches to -0.5 at large system size.

conjecture about the form of the right-hand side of (16):

$$P(\vec{k}) = e^{2\mu_0+\mu_1 F(\vec{k})}, \tag{18}$$

with μ_0 and μ_1 being the Lagrangian multiplier in the definition of the GGE (13) and $F(\vec{k})$ being a symmetric function of k_j,

$$F(\vec{k}) = \sum_{j=1}^{N} \ln \frac{k_j^2}{c^2} + \ln\left(\frac{k_j^2}{c^2} + \frac{1}{4}\right). \tag{19}$$

To verify this conjecture, we generated a series of DE at different sizes through MCBA, then randomly selected 2×10^3 states in each DE, and fitted these states by μ_0 and μ_1 using Eq. (18). Our results show that as the system size increases, Eq. (18) fits the results of the DE more accurately, see Fig. 4, which confirms the validity of the conjecture.

In order to find a formal solution for the operator $\hat{F}$ corresponding to F in (19), we can use the sequence of conserved operators $\hat{\mathcal{I}}_m$ in (17) obtained from the algebraic Bethe ansatz. For simplification, we set $y_j = \frac{4}{c^2}k_j^2$ and $\hat{O}_m = (\frac{2}{c})^{2m}\hat{\mathcal{I}}_{2m}$, then we have

$$O_m(\vec{k}) = \langle\vec{k}|\hat{O}_m|\vec{k}\rangle = \sum_{j=1}^{N} y_j^m, \tag{20}$$

and in the form of y_j (19) reads

$$F(\vec{k}) = \ln\left[2^{-4N}\prod_{j=1}^{N} y_j(1+y_j)\right]. \tag{21}$$

Notice that the polynomial $\prod_{j=1}^{N} y_j(1+y_j)$ can be expressed in terms of O_m in (20) by the Newton-Girard formula [92]. To be explicit, we denote the e_n with $n = 0, \ldots, N$ being the elementary symmetric polynomial of $y_1, \ldots, y_N$ of degree n. Then, we arrive at $\prod_{j=1}^{N} y_j(1+y_j) = e_N(e_0 + e_1 + \cdots + e_N)$, and each e_n can be expressed as a polynomial of O_m by formula

$$e_n = (-1)^n \sum_{\substack{m_1+2m_2+\cdots+nm_n=n \\ m_1\geqslant 0,\ldots,m_N\geqslant 0}} \prod_{j=1}^{N} \frac{(-O_j)^{m_j}}{m_j!\, j^{m_j}}. \tag{22}$$

If we replace the conserved quantities O_j by the conserved operators $O_j \to \hat{O}_j$ in (22), we can obtain the series of operators $e_n \to \hat{e}_n$. According to (21) we arrive at the expression of operator

$$\hat{F} = \ln[2^{-4N}\hat{e}_N(\hat{e}_0 + \hat{e}_1 + \cdots + \hat{e}_N)]. \tag{23}$$

The $\hat{e}_m$ are polynomials of $\hat{O}_m$, and therefore also polynomials of $\hat{\mathcal{I}}_m$, thus we can claim that the formula (23) gives the explicit form of the operator $\hat{F}$, satisfying $\langle\vec{k}|\hat{F}|\vec{k}\rangle = F(\vec{k})$. Clearly, the form of $\hat{F}$ is extremely complicated; it is obviously nonlocal, containing all higher-order conservation quantities given by the algebraic Bethe ansatz, so its physical meaning is utterly obscure. However, if we insist that the GGE should describe the steady postquench behavior of the system we are studying, $\hat{F}$ in (23) is still an appropriate choice for constructing the GGE, and it may even be the only one operator we need [see Eq. (18)] to determine the GGE (13), fitting well with the results of the DE by MCBA.

C. Remarks

In this section, we constructed the postquench DE of LLM through MCBA, and then by the analysis of the obtained data, we first verified the effectiveness of the quench TBA equation and then provided some analysis for the construction of GGE. There are two important remarks that need to be emphasized.

First, the $\rho(k)$ as a density distribution function has different meanings in MCBA and in the quench TBA equation. In MCBA, we regard all the roots of the BAE corresponding to all wave functions appearing in the diagonal ensemble as a set; this set gives a root distribution which is $\rho(k)$, while in the quench TBA equation, the meaning of $\rho(k)$ is a root distribution of one solution of BAE corresponding to the state with the maximum weight obtained by the saddle-point approximation. However, when we calculate the measurements of conserved quantities through density distributions, both methods share the same formula $\bar{I} = \int dk\rho(k)I(k)$ [31,71]. Thus, in this sense, at least statistically, these two $\rho(k)$s are equivalent, so in our calculation we did not specifically distinguish between them.

Second, despite our ability to reconstruct the DE effectively through MCBA, it remains a formidable challenge to extract additional physical insights from the data, particularly those pertaining to system correlations. The crux of this problem lies in our limited analytical understanding of the observable $\langle\vec{k}|\hat{O}|\vec{k}\rangle$ for the wave function $|\vec{k}\rangle$ provided by the BA, especially when $\hat{O}$ is the correlator. This long-standing challenge provides the impetus for the research undertaken in Sec. IV.

IV. CALCULATION OF THE CORRELATIONS BY MCBA

While research on the LLM (2) dates back to the 1960s when people first studied the model's ground state [72], energy spectrum [73], and finite temperature properties [76], the study of correlation functions in this model remains a challenging task. So far, there are only some analytical results related to impenetrable bosons [93,94] and long-range behavior [95,96]. In the past two decades, new numerical methods have been applied to the research of this problem [97–106]; these algorithms, being still in development, rely on the analytical results provided by the Bethe ansatz and require sophisticated numerical techniques with large-scale numerical computation [107,108], thus the problem of correlation functions in LLM has not been completely resolved to this day.

In this section, based on the Monte Carlo method, we propose an approach for calculating correlation functions using Bethe-ansatz wave functions. As discussed in Sec. II A, once the BAE (5) is solved, we directly arrive at the wave function of the eigenstate of the LLM, which reads

$$\Psi(x_1,\ldots,x_N)=\sum_{P\in S_N}A(P)\exp[ik_{P_1}x_1+\cdots+ik_{P_N}x_N] \quad (24)$$

in the sector $x_1<x_2<\cdots<x_N$, and values of the wave function in other sectors can be obtained through its symmetric property. The form of the wave function in (24) appears to be ideal, however, computation in this manner is nearly infeasible. For instance, when calculating the norm of the wave function, we immediately encounter

$$\begin{aligned}\langle\Psi|\Psi\rangle&=\int_0^1 dx_1,\ldots,dx_N\Psi^*(x_1,\ldots,x_N)\Psi(x_1,\ldots,x_N)\\&=N!\int_{0<x_1<\cdots<x_N<1}dx_1,\ldots,dx_N\Psi^*(x_1,\ldots,x_N)\Psi(x_1,\ldots,x_N)\\&=N!\int_{0<x_1<\cdots<x_N<1}dx_1,\ldots,dx_N\sum_{P,Q\in S_N}A(Q)^*A(P)\\&\quad\times\exp[i(k_{P_1}-k_{Q_1})x_1+\cdots+i(k_{P_N}-k_{Q_N})x_N].\end{aligned} \quad (25)$$

Notice that here we set $L=1$ as we do not consider the case of thermodynamic limit $L\to\infty$ in this section, and the $A(P), A(Q)$ can be evaluated by (4). Equation (25) is difficult to calculate for two reasons: one is that it involves multiple integrals, and the other is that it requires summation over $N!\times N!$ terms. The divergence speed of $N!\times N!$ is extremely fast; for instance, when $N=10$, it already exceeds 10^{13}, and such a scale of summation is almost impossible to accomplish on a computer. Therefore, so far, the limit size we have seen for direct calculation by wave function (24) is $N=7$ [102]. The same computational difficulties also arise when we attempt to calculate the correlation functions g_1 and g_2.

We use the first quantization definition of correlation functions $g_1(z)$ and $g_2(z)$, see Ref. [97], and expand them with the wave function (24):

$$\begin{aligned}g_1(z)&=\frac{1}{\langle\Psi|\Psi\rangle}\int_0^1 dx_2,\ldots,dx_N\Psi^*(0,\ldots,x_N)\Psi(z,\ldots,x_N)\\&=\frac{(N-1)!}{\langle\Psi|\Psi\rangle}\sum_{w=1}^{N}\int_{0<x_2<\cdots<x_w<z<x_{w+1}<\cdots<x_N<1}dx_2,\ldots,dx_N\,\Psi^*(0,x_2,\ldots,x_N)\Psi(x_2,\ldots,x_w,z,x_{w+1},\ldots,x_N)\\&=\frac{(N-1)!}{\langle\Psi|\Psi\rangle}\sum_{w=1}^{N}\sum_{P,Q\in S_N}\int_{0<x_2<\cdots<x_w<z<x_{w+1}<\cdots<x_N<1}dx_2,\ldots,dx_N\,A(Q)^*A(P)\\&\quad\times\exp[ik_{P_w}z+i(k_{P_1}-k_{Q_2})x_2+\cdots+i(k_{P_{w-1}}-k_{Q_w})x_{w-1}+i(k_{P_{w+1}}-k_{Q_{w+1}})x_{w+1}+\cdots+i(k_{P_N}-k_{Q_N})x_N]\end{aligned} \quad (26)$$

$$\begin{aligned}g_2(z)&=\frac{1}{\langle\Psi|\Psi\rangle}\int_0^1 dx_3,\ldots,dx_N\Psi^*(0,z,x_3,\ldots,x_N)\Psi(0,z,x_3,\ldots,x_N)\\&=\frac{(N-2)!}{\langle\Psi|\Psi\rangle}\sum_{w=1}^{N-1}\int_{0<x_3<\cdots<x_{w+1}<z<x_{w+2}<\cdots<x_N<1}dx_3,\ldots,dx_N\,|\Psi(0,x_3,\ldots,x_{w+1},z,x_{w+2},\ldots,x_N)|^2\\&=\frac{(N-1)!}{\langle\Psi|\Psi\rangle}\sum_{w=1}^{N-1}\sum_{P,Q\in S_N}\int_{0<x_3<\cdots<x_{w+1}<z<x_{w+2}<\cdots<x_N<1}dx_3,\ldots,dx_N\,A(Q)^*A(P)\exp[i(k_{P_2}-k_{Q_2})x_3+\cdots\\&\quad+i(k_{P_w}-k_{Q_w})x_{w+1}+i(k_{P_{w+1}}-k_{Q_{w+1}})z+i(k_{P_{w+2}}-k_{Q_{w+2}})x_{w+2}+\cdots+i(k_{P_N}-k_{Q_N})x_N].\end{aligned} \quad (27)$$

Subsequently, we dissect these two complicated expressions into their summation and integration components, and proceed to simplify each of them. In order to achieve this, we introduce the notation g_{PQ}, $g^{(1)}_{PQ}(z)$ and $g^{(1)}_{PQ}(z)$ by

$$g_{PQ}=A(Q)^*A(P)\int_{0<x_1<\cdots<x_N<1}dx_1,\ldots,dx_N\exp[i(k_{P_1}-k_{Q_1})x_1+\cdots+i(k_{P_N}-k_{Q_N})x_N], \quad (28)$$

$$g^{(1)}_{PQ}(z) = A(Q)^* A(P) \sum_{w=1}^{N} \int_{0<x_2<\cdots<x_w<z<x_{w+1}<\cdots<x_N<1} dx_2, \ldots, dx_N \exp[ik_{P_w} z + i(k_{P_1} - k_{Q_2})x_2 + \cdots + i(k_{P_{w-1}} - k_{Q_w})x_w + i(k_{P_{w+1}} - k_{Q_{w+1}})x_{w+1} + \cdots + i(k_{P_N} - k_{Q_N})x_N], \tag{29}$$

$$g^{(2)}_{PQ}(z) = A(Q)^* A(P) \sum_{w=1}^{N-1} \int_{0<x_3<\cdots<x_{w+1}<z<x_{w+2}<\cdots<x_N<1} dx_3, \ldots, dx_N \exp[i(k_{P_2} - k_{Q_2})x_3 + \cdots + i(k_{P_w} - k_{Q_w})x_{w+1} + i(k_{P_{w+1}} - k_{Q_{w+1}})z + i(k_{P_{w+2}} - k_{Q_{w+2}})x_{w+2} + \cdots + i(k_{P_N} - k_{Q_N})x_N], \tag{30}$$

which are in charge with the calculation of the integral part in Eqs. (25), (26), and (27), respectively. Utilizing these symbols, we can express the correlation functions by summations

$$g_1(z) = \frac{1}{N} \frac{\sum_{P,Q\in S_N} g^{(1)}_{PQ}(z)}{\sum_{P,Q\in S_N} g_{PQ}}, \tag{31}$$

$$g_2(z) = \frac{1}{N(N-1)} \frac{\sum_{P,Q\in S_N} g^{(2)}_{PQ}(z)}{\sum_{P,Q\in S_N} g_{PQ}}. \tag{32}$$

An important observation is that the integrals in Eqs. (28)–(30) do have analytical expressions. A general result of this kind of integral reads

$$\int_{0<x_1<\cdots<x_N<1} dx_1, \ldots, dx_N \exp[i(k_1 x_1 + \cdots + k_N x_N)] = g[k_1 + \cdots + k_N, k_2 + \cdots + k_N, \ldots, k_N, 0] \tag{33}$$

with the symmetric function $g[\chi_1, \ldots, \chi_N]$ defined by

$$g[\chi_1, \ldots, \chi_N] = \sum_{n_1,\cdots,n_N=0}^{\infty} \frac{(i\chi_1)^{n_1}(i\chi_2)^{n_2}\cdots(i\chi_N)^{n_N}}{(n_1 + n_2 + \cdots + n_N)!}. \tag{34}$$

The function above has nice properties for real variables; it is smooth and bounded, with iterative relation

$$g[\chi_1, \chi_2, \ldots, \chi_N] = \frac{g[\chi_1, \chi_3, \ldots, x_N] - g[\chi_2, \chi_3, \ldots, x_N]}{\chi_1 - \chi_2}, \tag{35}$$

and when all the variables are equal, we have

$$g[\chi_1 = a, \chi_2 = a, \ldots, \chi_N = a] = \frac{i^{N-1}}{(N-1)!} e^{ia}. \tag{36}$$

Notice that $g[\chi] = e^{i\chi}$ is the case $N = 1$ in (36). With the help of (35) and (36), we can numerically obtain the value of any $g[\chi_1, \ldots, \chi_N]$ with real variables in polynomial steps [more specifically, the time complexity of calculating g is $O(N^2)$]. Despite the potential problem associated with differentiation in (35), we find these pseudosingularities will not present principal difficulties when handled carefully due to the smoothness and boundedness of the function $g[\chi_1, \ldots, \chi_N]$ itself. Therefore, the difficulty of multi-integral calculation has been numerically resolved. With the help of (33), (35), and (36), we are able to calculate g_{PQ}, $g^{(1)}_{PQ}(z)$, and $g^{(2)}_{PQ}(z)$ in (28)–(30) for any given P, Q, and z in an economical manner.

We are now in the position to calculate the correlation function (26) and (27). We observe that $|g[\chi_1, \chi_2, \ldots, \chi_N]|$ attains its maximum value if and only if all the χ_j take the same value. This implies that the absolute value of g_{PQ} in (28) has a maximum when P and Q are equal. Further, we notice, roughly speaking, that the absolute value of g_{PQ} is larger when P and Q are "closer." (To put it concretely, the closer P and Q, the fewer exchange operations are needed to link each other.) The same phenomenon also occurs in the calculation of $g^{(1)}_{PQ}(z)$ and $g^{(2)}_{PQ}(z)$ in (29) and (30). This inspires us to use $|g_{PQ}|$ to perform importance sampling in the nearly infinite phase space $S_N \times S_N$ of $\{P, Q\}$. To accomplish this idea, we introduce the effective partition function

$$Z = \sum_{P,Q\in S_N} |g_{PQ}|^\delta; \tag{37}$$

this partition function corresponds to an ensemble giving a probability $Z^{-1}|g_{PQ}|^\delta$ to each point in the phase space $S_N \times S_N$. Here, the δ in (37) is a positive parameter which can tune the transition rate in the Monte Carlo algorithm that will be discussed below. Under this setup, we are able to express $g_1(z)$ and $g_2(z)$ in (31) and (32) in the form of ensemble averages:

$$g_1(z) = \frac{1}{N} \frac{\langle g^{(1)}_{PQ}(z)/|g_{PQ}|^\delta \rangle_Z}{\langle g_{PQ}/|g_{PQ}|^\delta \rangle_Z} = \frac{1}{N} \frac{Z^{-1} \sum_{P,Q\in S_N} \frac{g^{(1)}_{PQ}(z)}{|g_{PQ}|^\delta} |g_{PQ}|^\delta}{Z^{-1} \sum_{P,Q\in S_N} \frac{g_{PQ}}{|g_{PQ}|^\delta} |g_{PQ}|^\delta}, \tag{38}$$

$$g_2(z) = \frac{1}{N(N-1)} \frac{\langle g^{(2)}_{PQ}(z)/|g_{PQ}|^\delta \rangle_Z}{\langle g_{PQ}/|g_{PQ}|^\delta \rangle_Z} = \frac{1}{N(N-1)} \frac{Z^{-1} \sum_{P,Q\in S_N} \frac{g^{(2)}_{PQ}(z)}{|g_{PQ}|^\delta} |g_{PQ}|^\delta}{Z^{-1} \sum_{P,Q\in S_N} \frac{g_{PQ}}{|g_{PQ}|^\delta} |g_{PQ}|^\delta}. \tag{39}$$

The expressions in (38) and (39) have paved the way for MCBA calculations, and the algorithm is designed as follows. We begin with any $\{P, Q\}$ in the phase space $S_N \times S_N$, and then do the random walk in this space corresponding to the probability $Z^{-1}|g_{PQ}|^\delta$. To achieve the random walk, we generate a candidate by randomly changing P or Q by randomly generated exchange operation, and then use the Metropolis-Hastings algorithm to determine whether to accept or reject this candidate. After a sufficient number of steps, we can calculate the numerators and denominators of (38) and (39), respectively, provide estimates and errors, and thus solve for $g_1(z)$ and $g_2(z)$.

In Fig. 5, we present the result of the correlation functions for $N = 5$, where the wave function is chosen to be the first excitation states. We compare our numerical results to the

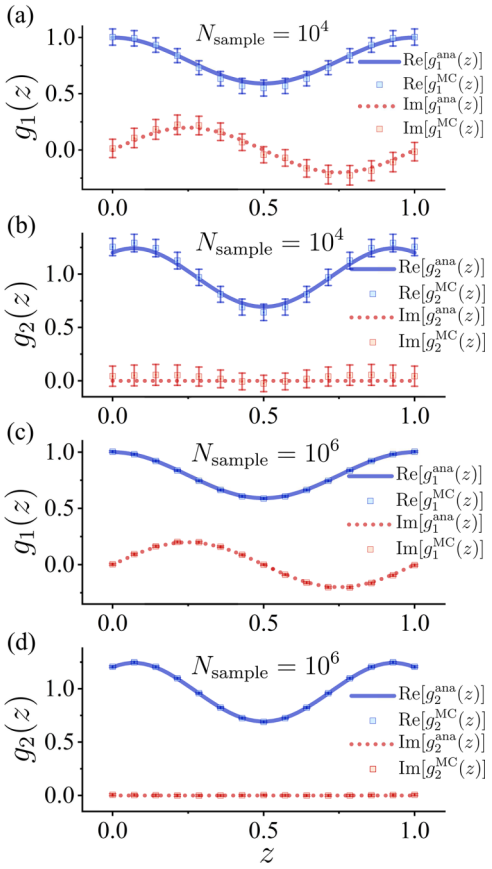

FIG. 5. The correlation function $g_1(z)$ and $g_2(z)$ for $N = 5$ and first excitation state of the Hamiltonian (2), with $L = 1$ and $c = 1.0$. The scatters with error bars are results obtained by the MCBA, where in (a) and (b) the number of sampling in the MCBA algorithm is 10^4, while in (c) and (d) it is 10^6. The blue solid lines correspond to the real parts and the red dash lines to the imaginary parts of the correlation functions obtained by analytical calculation.

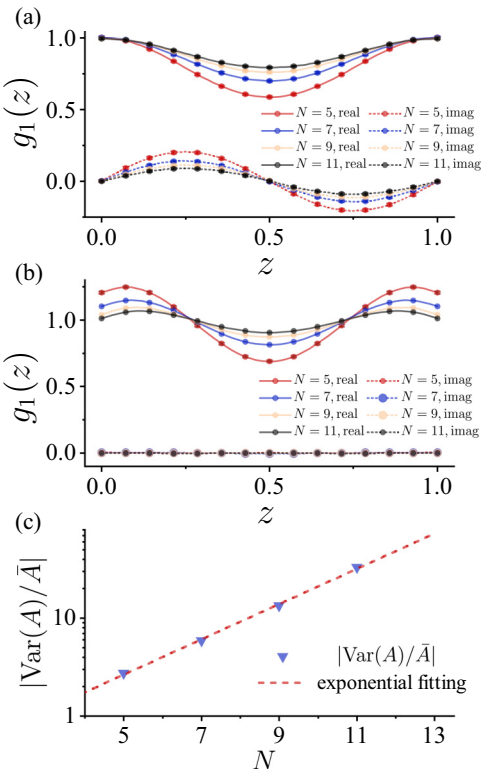

FIG. 6. (a and b) The correlation function $g_1(z)$ and $g_2(z)$ for $N = 5, 7, 9$, and 11, with first excitation state of the Hamiltonian (2). Here, we set $L = 1$ and $c = 1.0$. The scatters with error bars are results obtained by the MCBA, and the solid lines and dash lines correspond to the real and imaginary part of the correlation functions, respectively. (c) The absolute value of the ratio of the variance to the mean of the random variable $A = g_{PQ}/|g_{PQ}|$ as N increases. The exponential divergence of this parameter indicates the presence of the sign problem in Monte Carlo calculations.

straightforward analytical calculation by (26) and (27) (when N is small, direct calculation of the correlation functions is feasible). The results show a good agreement between the MCBA and the analytical calculation. We set $\delta = 1.0$ in (37) here and below for simplicity.

In Fig. 6, we present the result of the correlation function for $N = 5, 7, 9$, and 11, where again the wave function is chosen to be the first excitation state. Our results show the well-behaved convergence of the MCBA.

However, when we aim to perform calculations for larger-size systems, we encounter the sign problem in the QMC algorithm. In Table I, we show the number of samples we have generated by MCBA for plotting Fig. 6. It shows that as N increases, the number of samples we used to achieve convergent results increases exponentially. To study this divergence behavior, we calculated the absolute value of the ratio of the variance to the mean of the random variable $A = g_{PQ}/|g_{PQ}|^{\delta}$ in the denominators of (38) and (39), the results of which are presented in Fig. 6(c). It shows that the ratio of the variance to the mean of A exhibits exponential divergence as N increases, confirming that we indeed need an exponentially divergent number of samples to obtain convergent results.

TABLE I. The number of samples we used for different system size in Fig. 6.

N	5	7	9	11
N_{sample}	2×10^6	5×10^6	4×10^7	2×10^8

The sign problem arises inherently from the algorithm itself. Referring to Eqs. (38) and (39), where their denominators are considered, our computation essentially involves sampling points on the unit circle in the complex plane. If the true expectation value in the denominator is close to zero, according to the uncertainty propagation formula, the uncertainties calculated in the denominator will be magnified greatly, making the convergence of the computation difficult. Fundamentally, this problem arises from the fact that the samples being drawn do not have a definite sign, leading to positive and negative cancellations in the numerical simulations. This is essentially the sign problem encountered in QMC calculations, thus we refer to it as the "sign problem."

Notice that our method significantly differs from a range of well-established Monte Carlo methods such as variational Monte Carlo (VMC) [58,59], path integral MC (PIMC) [109]

or diffusion MC (DMC) [110,111]. Our method essentially employs the Monte Carlo technique to compute the wave function (24) given by the Bethe ansatz, attempting to use the exact solution to provide more physical information beyond just the spectrum, which is a challenging problem in the study of quantum integrable models [75]. Although this approach currently appears to have some difficulties, its advantages are also clear. Compared to VMC, it does not rely on trial wave functions, thus its error is solely due to statistical uncertainty without systematic error; compared to DMC, PIMC, or other well-developed variational methods (the continuous matrix product state algorithm [112,113] for instance), it can more easily calculate arbitrary system eigenstates, such as the first excited state information that we have calculated as an example in this paper.

To summarize, despite encountering the sign problem while trying to calculate larger-size systems, we have successfully validated the feasibility of the Monte Carlo algorithm in calculating wave functions, and our algorithm has already surpassed the current size limit for direct wave-function calculation through exact solution obtained by Bethe ansatz [29,102]. In fact, our algorithm still has considerable room for improvement, as there is a high degree of freedom in selecting the partition function (37). If we can select the partition function more appropriately based on the characteristics of the data, we should obtain better convergence. We hope to make further improvements to this algorithm in future work.

V. SUMMARY AND OUTLOOK

In the present study, we have systematically incorporated the Monte Carlo methodology into the exact solution from the Bethe ansatz, thereby facilitating the first-principles construction and computation of statistical ensembles. This approach has enabled us to explore the intricacies of both equilibrium and nonequilibrium states within integrable models. Utilizing the probabilities of states in the statistical ensemble provided by the analytical results of the exact solutions, and in conjunction with the Metropolis-Hastings algorithm, we have successfully reconstructed the statistical ensemble. This has laid the groundwork for our analysis of the equilibrium and nonequilibrium properties of the quantum integrable system.

Our numerical findings corroborate the validation of the (quench) TBA equations, which were derived based on the quasi-particle picture and saddle-point approximation. Moreover, our explorations into the diagonal ensemble postquench yielded a concrete conjecture in the form of the generalized Gibbs ensemble (GGE).

We also extended the use of the Monte Carlo Bethe ansatz to the computation of correlation functions in Sec. IV. Despite encountering the well-known sign problem inherent in quantum Monte Carlo algorithms when dealing with larger sizes, our findings reaffirm the efficacy of the MCBA method within the context of few-body problems. Notably, the computational scalability achieved in our study has transcended the prevailing limitations associated with studying correlation functions via direct wave-function calculations. As a prospect, coupled with the method of ensemble simulations through Monte Carlo discussed in detail in Secs. II and III, our algorithm holds the potential to compute the correlation functions of quantum integrable systems in equilibrium or steady states.

The Monte Carlo method and the Bethe ansatz are two mature methodologies that have been developed over a long period of time for the study of many-body physics, yet research combining these two methods remains rare to this day. Therefore, our work provides a different approach. We have also encountered certain difficulties in our current research. Firstly, as discussed in Sec. III C, having fully constructed the statistical ensemble through numerical calculations, we still find it challenging to obtain richer physical information beyond conserved quantities, especially information related to correlation functions. This difficulty arises from the current lack of sufficient analytical results regarding the correlation of Bethe-ansatz wave functions. Secondly, when we applied the MCBA to the calculation of correlation functions, we encountered the typical sign problem inherent in Monte Carlo algorithms. These two challenges present demands for our future research. We hope to delve deeper into the study of the Bethe ansatz, exploring possible analytical forms of correlation functions. On the other hand, we anticipate that leveraging existing research on the Monte Carlo algorithm will help us find ways to reduce the negative impact of the sign problem in the calculation of correlation functions.

ACKNOWLEDGMENTS

This work is supported by the National Natural Science Foundation of China under Grants No. 12274419, No. 12104372, and No. 12134015, and the CAS Project for Young Scientists in Basic Research under Grant No. YSBR-055.

[1] J. M. Deutsch, Phys. Rev. A **43**, 2046 (1991).
[2] M. Srednicki, Phys. Rev. E **50**, 888 (1994).
[3] M. Rigol, V. Dunjko, and M. Olshanii, Nature (London) **452**, 854 (2008).
[4] A. Polkovnikov, K. Sengupta, A. Silva, and M. Vengalattore, Rev. Mod. Phys. **83**, 863 (2011).
[5] R. Nandkishore and D. A. Huse, Annu. Rev. Condens. Matter Phys. **6**, 15 (2015).
[6] F. H. L. Essler and M. Fagotti, J. Stat. Mech.: Theory Exp. (2016) 064002.
[7] V. Alba and P. Calabrese, Proc. Natl. Acad. Sci. **114**, 7947 (2017).
[8] K. Sengupta, S. Powell, and S. Sachdev, Phys. Rev. A **69**, 053616 (2004).
[9] J. Berges, S. Borsányi, and C. Wetterich, Phys. Rev. Lett. **93**, 142002 (2004).
[10] S. Hofferberth, I. Lesanovsky, B. Fischer, T. Schumm, and J. Schmiedmayer, Nature (London) **449**, 324 (2007).
[11] I. Bloch, J. Dalibard, and W. Zwerger, Rev. Mod. Phys. **80**, 885 (2008).
[12] M. Gring, M. Kuhnert, T. Langen, T. Kitagawa, B. Rauer, M. Schreitl, I. Mazets, D. A. Smith, E. Demler, and J. Schmiedmayer, Science **337**, 1318 (2012).

[13] J.-P. Brantut, C. Grenier, J. Meineke, D. Stadler, S. Krinner, C. Kollath, T. Esslinger, and A. Georges, Science **342**, 713 (2013).

[14] T. Langen, R. Geiger, M. Kuhnert, B. Rauer, and J. Schmiedmayer, Nat. Phys. **9**, 640 (2013).

[15] C. Gross and I. Bloch, Science **357**, 995 (2017).

[16] M. Prüfer, T. V. Zache, P. Kunkel, S. Lannig, A. Bonnin, H. Strobel, J. Berges, and M. K. Oberthaler, Nat. Phys. **16**, 1012 (2020).

[17] F. Carollo, F. M. Gambetta, K. Brandner, J. P. Garrahan, and I. Lesanovsky, Phys. Rev. Lett. **124**, 170602 (2020).

[18] J. Marino, M. Eckstein, M. S. Foster, and A. M. Rey, Rep. Prog. Phys. **85**, 116001 (2022).

[19] M. T. Mitchison, A. Purkayastha, M. Brenes, A. Silva, and J. Goold, Phys. Rev. A **105**, L030201 (2022).

[20] X.-W. Guan and P. He, Rep. Prog. Phys. **85**, 114001 (2022).

[21] J.-S. Caux and R. M. Konik, Phys. Rev. Lett. **109**, 175301 (2012).

[22] G. Mussardo, Phys. Rev. Lett. **111**, 100401 (2013).

[23] J.-S. Caux and F. H. L. Essler, Phys. Rev. Lett. **110**, 257203 (2013).

[24] B. Pozsgay, M. Mestyán, M. A. Werner, M. Kormos, G. Zaránd, and G. Takács, Phys. Rev. Lett. **113**, 117203 (2014).

[25] B. Wouters, J. De Nardis, M. Brockmann, D. Fioretto, M. Rigol, and J.-S. Caux, Phys. Rev. Lett. **113**, 117202 (2014).

[26] E. Ilievski, J. De Nardis, B. Wouters, J.-S. Caux, F. H. L. Essler, and T. Prosen, Phys. Rev. Lett. **115**, 157201 (2015).

[27] R. Mondaini and M. Rigol, Phys. Rev. A **92**, 041601(R) (2015).

[28] J. Eisert, M. Friesdorf, and C. Gogolin, Nat. Phys. **11**, 124 (2015).

[29] J. C. Zill, T. M. Wright, K. V. Kheruntsyan, T. Gasenzer, and M. J. Davis, Phys. Rev. A **91**, 023611 (2015).

[30] B. Bertini, M. Collura, J. De Nardis, and M. Fagotti, Phys. Rev. Lett. **117**, 207201 (2016).

[31] O. A. Castro-Alvaredo, B. Doyon, and T. Yoshimura, Phys. Rev. X **6**, 041065 (2016).

[32] J.-S. Caux, J. Stat. Mech.: Theory Exp. (2016) 064006.

[33] L. Vidmar and M. Rigol, J. Stat. Mech.: Theory Exp. (2016) 064007.

[34] B. Opanchuk and P. D. Drummond, Phys. Rev. A **96**, 053628 (2017).

[35] J. De Nardis, D. Bernard, and B. Doyon, Phys. Rev. Lett. **121**, 160603 (2018).

[36] K. Mallayya, M. Rigol, and W. De Roeck, Phys. Rev. X **9**, 021027 (2019).

[37] S. Wang, X. Yin, Y.-Y. Chen, Y. Zhang, and X.-W. Guan, J. Phys. A: Math. Theor. **53**, 464002 (2020).

[38] B. Bertini, F. Heidrich-Meisner, C. Karrasch, T. Prosen, R. Steinigeweg, and M. Žnidarič, Rev. Mod. Phys. **93**, 025003 (2021).

[39] H.-B. Chen and Y.-N. Chen, Sci. Rep. **11**, 10046 (2021).

[40] K. Mallayya and M. Rigol, Phys. Rev. B **104**, 184302 (2021).

[41] V. Alba, B. Bertini, M. Fagotti, L. Piroli, and P. Ruggiero, J. Stat. Mech.: Theory Exp. (2021) 114004.

[42] D. Ruelle, J. Stat. Phys. **98**, 57 (2000).

[43] M. Rigol, V. Dunjko, V. Yurovsky, and M. Olshanii, Phys. Rev. Lett. **98**, 050405 (2007).

[44] B. Doyon, Commun. Math. Phys. **351**, 155 (2017).

[45] B. Pozsgay, E. Vernier, and M. A. Werner, J. Stat. Mech.: Theory Exp. (2017) 093103.

[46] A. C. Cassidy, C. W. Clark, and M. Rigol, Phys. Rev. Lett. **106**, 140405 (2011).

[47] C. Gramsch and M. Rigol, Phys. Rev. A **86**, 053615 (2012).

[48] T. Langen, S. Erne, R. Geiger, B. Rauer, T. Schweigler, M. Kuhnert, W. Rohringer, I. E. Mazets, T. Gasenzer, and J. Schmiedmayer, Science **348**, 207 (2015).

[49] M. Schemmer, I. Bouchoule, B. Doyon, and J. Dubail, Phys. Rev. Lett. **122**, 090601 (2019).

[50] A. Bastianello, A. De Luca, B. Doyon, and J. De Nardis, Phys. Rev. Lett. **125**, 240604 (2020).

[51] A. Schuckert and M. Knap, Phys. Rev. Res. **2**, 043315 (2020).

[52] J. Durnin, M. J. Bhaseen, and B. Doyon, Phys. Rev. Lett. **127**, 130601 (2021).

[53] F. Møller, C. Li, I. Mazets, H.-P. Stimming, T. Zhou, Z. Zhu, X. Chen, and J. Schmiedmayer, Phys. Rev. Lett. **126**, 090602 (2021).

[54] Q.-Q. Wang, S.-J. Tao, W.-W. Pan, Z. Chen, G. Chen, K. Sun, J.-S. Xu, X.-Y. Xu, Y.-J. Han, C.-F. Li, and G.-C. Guo, Light Sci. Appl. **11**, 194 (2022).

[55] K. Huang, *Introduction to Statistical Physics* (CRC Press, Boca Raton, 2009).

[56] L. D. Landau and E. M. Lifshitz, *Statistical Physics* (Elsevier, New York, 2013), Vol. 5.

[57] A. W. Sandvik and J. Kurkijärvi, Phys. Rev. B **43**, 5950 (1991).

[58] M. P. Nightingale and C. J. Umrigar, *Quantum Monte Carlo Methods in Physics and Chemistry* (Springer Science & Business Media, Heidelberg, 1998).

[59] W. M. C. Foulkes, L. Mitas, R. J. Needs, and G. Rajagopal, Rev. Mod. Phys. **73**, 33 (2001).

[60] B. M. Austin, D. Y. Zubarev, and W. A. J. Lester, Chem. Rev. **112**, 263 (2012).

[61] J. Carlson, S. Gandolfi, F. Pederiva, S. C. Pieper, R. Schiavilla, K. E. Schmidt, and R. B. Wiringa, Rev. Mod. Phys. **87**, 1067 (2015).

[62] S. Herbert, Quantum **6**, 823 (2022).

[63] J. Gubernatis, N. Kawashima, and P. Werner, *Quantum Monte Carlo Methods* (Cambridge University Press, Cambridge, 2016).

[64] F. Becca and S. Sorella, *Quantum Monte Carlo Approaches for Correlated Systems* (Cambridge University Press, Cambridge, 2017).

[65] D. Ceperley and B. Alder, Science **231**, 555 (1986).

[66] M. Suzuki, *Quantum Monte Carlo Methods in Condensed Matter Physics* (World Scientific, Singapore, 1993).

[67] N. Metropolis, A. W. Rosenbluth, M. N. Rosenbluth, A. H. Teller, and E. Teller, J. Chem. Phys. **21**, 1087 (1953).

[68] S.-J. Gu, N. M. R. Peres, and Y.-Q. Li, Eur. Phys. J. B **48**, 157 (2005).

[69] F. Buccheri, A. De Luca, and A. Scardicchio, Phys. Rev. B **84**, 094203 (2011).

[70] A. Faribault and D. Schuricht, Phys. Rev. Lett. **110**, 040405 (2013).

[71] V. Alba and P. Calabrese, J. Stat. Mech.: Theory Exp. (2016) 043105.

[72] E. H. Lieb and W. Liniger, Phys. Rev. **130**, 1605 (1963).

[73] E. H. Lieb, Phys. Rev. **130**, 1616 (1963).

[74] Y.-Z. Jiang, Y.-Y. Chen, and X.-W. Guan, Chin. Phys. B **24**, 050311 (2015).

[75] V. E. Korepin, N. M. Bogoliubov, and A. G. Izergin, *Quantum Inverse Scattering Method and Correlation Functions* (Cambridge University Press, Cambridge, 1997).

[76] C. N. Yang and C. P. Yang, J. Math. Phys. **10**, 1115 (1969).

[77] Z.-S. Yuan, X.-W. Guan, and J.-W. Pan, in *A Festschrift in Honor of the C N Yang Centenary* (World Scientific, Singapore, 2022), pp. 263–280.

[78] L. D. Landau, Sov. Phys. JETP **8**, 70 (1959).

[79] J. Dukelsky, S. Pittel, and G. Sierra, Rev. Mod. Phys. **76**, 643 (2004).

[80] M. Bortz and J. Stolze, Phys. Rev. B **76**, 014304 (2007).

[81] X.-W. Guan, M. T. Batchelor, and M. Takahashi, Phys. Rev. A **76**, 043617 (2007).

[82] M. Takahashi, *Thermodynamics of One-Dimensional Solvable Models* (Cambridge University Press, 1999).

[83] J. De Nardis, B. Wouters, M. Brockmann, and J.-S. Caux, Phys. Rev. A **89**, 033601 (2014).

[84] M. Kormos, M. Collura, and P. Calabrese, Phys. Rev. A **89**, 013609 (2014).

[85] B. M. Wouters, *The Quench Action Approach to Out-of-Equilibrium Quantum Integrable Models* (Universiteit van Amsterdam [Host], 2015).

[86] V. Gritsev, T. Rostunov, and E. Demler, J. Stat. Mech.: Theory Exp. (2010) P05012.

[87] H. E. Daniels, Ann. Math. Stat. **2**5, 631 (1954).

[88] B. Davies and V. E. Korepin, arXiv:1109.6604 [cond-mat, physics:math-ph].

[89] G. Brandino, J.-S. Caux, and R. Konik, arXiv:1301.0308 [cond-mat].

[90] M. Kormos, A. Shashi, Y.-Z. Chou, J.-S. Caux, and A. Imambekov, Phys. Rev. B **88**, 205131 (2013).

[91] J. Mossel and J.-S. Caux, New J. Phys. **14**, 075006 (2012).

[92] R. Séroul, *Programming for Mathematicians* (Springer Science & Business Media, Heidelberg, 2012).

[93] H. G. Vaidya and C. A. Tracy, Phys. Rev. Lett. **42**, 3 (1979).

[94] A. Lenard, J. Math. Phys. **5**, 930 (1964).

[95] F. D. M. Haldane, Phys. Rev. Lett. **47**, 1840 (1981).

[96] M. Schwartz, Phys. Rev. B **15**, 1399 (1977).

[97] G. E. Astrakharchik and S. Giorgini, J. Phys. B: At. Mol. Opt. Phys. **39**, S1 (2006).

[98] J.-S. Caux, P. Calabrese, and N. A. Slavnov, J. Stat. Mech.: Theory Exp. (2007) P01008.

[99] B. Pozsgay, J. Stat. Mech.: Theory Exp. (2011) P11017.

[100] L. Piroli and P. Calabrese, J. Phys. A: Math. Theor. **48**, 454002 (2015).

[101] J. De Nardis and M. Panfil, SciPost Phys. **1**, 015 (2016).

[102] J. C. Zill, T. M. Wright, K. V. Kheruntsyan, T. Gasenzer, and M. J. Davis, New J. Phys. **18**, 045010 (2016).

[103] H.-H. Chen, Phys. Lett. B **808**, 135631 (2020).

[104] S. Cheng, Y.-Y. Chen, X.-W. Guan, W.-L. Yang, R. Mondaini, and H.-Q. Lin, arXiv:2209.15221 [cond-mat, physics:quant-ph].

[105] S. Cheng, Y.-Y. Chen, X.-W. Guan, W.-L. Yang, and H.-Q. Lin, arXiv:2211.00282 [cond-mat].

[106] R.-T. Li, S. Cheng, Y.-Y. Chen, and X.-W. Guan, J. Phys. A: Math. Theor. **56**, 335204 (2023).

[107] J.-S. Caux, J. Math. Phys. **50**, 095214 (2009).

[108] A. J. J. M. de Klerk and J.-S. Caux, SciPost Phys. Core **6**, 039 (2023).

[109] C. M. Herdman, P.-N. Roy, R. G. Melko, and A. Del Maestro, Phys. Rev. B **94**, 064524 (2016).

[110] G. E. Astrakharchik, D. M. Gangardt, Yu. E. Lozovik, and I. A. Sorokin, Phys. Rev. E **74**, 021105 (2006).

[111] G. E. Astrakharchik and S. Giorgini, Phys. Rev. A **68**, 031602(R) (2003).

[112] S. Dutta, A. Buyskikh, A. J. Daley, and E. J. Mueller, Phys. Rev. Lett. **128**, 230401 (2022).

[113] J. Rincón, M. Ganahl, and G. Vidal, Phys. Rev. B **92**, 115107 (2015).